Electronic Materials Letters (2022) 18:113–128
https://doi.org/10.1007/s13391-021-00333-5

REVIEW PAPER

Epitaxial Growth of Alpha Gallium Oxide Thin Films on Sapphire Substrates for Electronic and Optoelectronic Devices: Progress and Perspective

Duyoung Yang[1] · Byungsoo Kim[1] · Tae Hoon Eom[1] · Yongjo Park[2] · Ho Won Jang[1,2]

Received: 20 December 2021 / Accepted: 21 December 2021 / Published online: 6 January 2022

Abstract

The demand for high-efficient and robust power semiconductors in harsh environments such as high temperature and high voltage has been enlarged with the fast development of the industry. Gallium oxide (Ga_2O_3) with a larger bandgap energy of 4.8–5.3 eV than Si, SiC, and GaN is a promising material suitable for next-generation power devices. Among the Ga_2O_3's phases, corundum structured α-Ga_2O_3 has attracted much attention, benefiting from the epitaxial growth on cheap sapphire substrate and the existence of p-type materials with the same crystal structure. This paper comprehensively reviews the progress on the epitaxial growth of α-Ga_2O_3 thin films and the fabrication of α-Ga_2O_3-based electronic and optoelectronic devices. First, state-of-the-art technologies for improving the crystal quality of α-Ga_2O_3 depending on growth methods are presented. Secondly, the current research level of growth of n-type doped α-Ga_2O_3 is comprehended. Finally, the recent progress of electronic and optoelectronic devices, including Schottky diodes, field-effect transistors, and solar-blind photodetectors, is summarized.

Graphical abstract

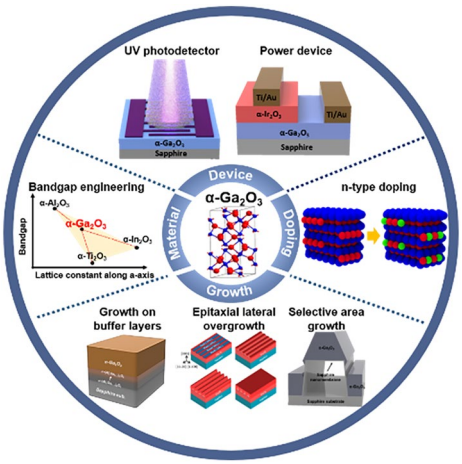

Keywords Alpha gallium oxide · Epitaxial growth · Doping · Power device · Solar-blind photodetector

✉ Ho Won Jang
hwjang@snu.ac.kr

[1] Department of Materials Science and Engineering, Research Institute of Advanced Materials, Seoul National University, Seoul 08826, Republic of Korea

[2] Advanced Institute of Convergence Technology, Seoul National University, Suwon 16229, Republic of Korea

1 Introduction

With the fast development of the industry, energy consumption has remarkably increased [1]. To cope with the rising energy consumption, the electricity generation is increasing,

but it is inevitably accompanied by combustion of fossil fuels. The combustion of the fuels leads to a large amount of greenhouse gas emissions, which is the main reason for environmental issues such as global warming and climate change. One of the strategies for mitigating these issues is to minimize the combustion by using electrical energy efficiently. Electrical energy is lost during the continuous conversion process that happens from generation to consumption, therefore reducing the loss is critical to using energy efficiently. Because it is the power device that executes the power conversion process through switching or rectification, it is important to improve its efficiency. Conventional power devices have been generally manufactured of Si, but its narrow bandgap results in significant leakage current, lowering switching efficiency of the devices. To address this issue, researchers began using wide bandgap (WBG) materials such as silicon carbide (SiC) [2, 3], and gallium nitride (GaN) [4] in power devices. It was reported that SiC devices had lower switching losses than Si devices across all temperature and frequency ranges due to its large bandgap energy [5]. Wide bandgap materials also have large breakdown fields, making it easier to make high-voltage devices and helping with miniaturization by reducing the drift layer. Researchers' interest in prospective materials for the development of next-generation power devices is expanding as the devices made of the WBG materials become commercialized. Gallium oxide (Ga_2O_3) is known as a representative material because it has a larger bandgap energy and breakdown field than commercialized WBG materials [6]. The material, especially β-Ga_2O_3, has a Baliga's figures of merit ($BFOM = \varepsilon \bullet \mu \bullet E_C^3$ where ε: dielectric constant, μ: carrier mobility, and E_C: breakdown field) value that is 5.6 and 2.2 times higher than SiC and GaN, respectively [1, 7]. Furthermore, beta gallium oxide allows for n-type doping across a wide range of carrier concentrations from 10^{16} to $10^{19}/cm^3$, making it more favorable for device development than materials with higher bandgap energies that are harder to dope [8]. Therefore, Ga_2O_3 with high bandgap energy, breakdown field, and doping controllability can be the most promising candidate for the fabrication of electronic and optoelectronic devices, notwithstanding the issues with p-type doping.

Ga_2O_3 crystals can exist in various polymorphs such as α [9], β [10, 11], γ [12], ε [13], κ [13, 14], and δ [15]. Among the five polymorphs, β-Ga_2O_3 is the thermodynamically most stable, which can be fabricated as a substrate through conventional solution-based technologies such as floating-zone (FZ) [16], edge-defined film-fed growth (EFG) [17], and Czochralski [18] methods. However, the commercialized size of the substrate still remains in 4-inch, and the price is higher than other conventional substrates such as Si and sapphire. Furthermore, the crystal defects like pits, voids, and twin defects still are obstacles to the fabrication of large-scale growth techniques [19].

On the other hand, α-Ga_2O_3 has attracted researchers' interest as it is possible to grow single-crystalline α-Ga_2O_3 thin films without any rotational domains on cheap sapphire substrates. The epitaxial growth is due to the same rhombohedral corundum crystal structure. Although β-Ga_2O_3 can grow on sapphire epitaxially, it was reported that crystal asymmetry between β-Ga_2O_3 and α-Al_2O_3 results in two distinct textures of the $(\bar{2}01)$ and (101) planes of the monoclinic phase as well as in-plane rotational domains [20, 21]. The structural problems can limit the β-Ga_2O_3 properties. Also, the α phase has the largest bandgap energy among the polymorphs, ranging from 5.0 to 5.3 eV, resulting in an increased BFOM value that is 2.7 times that of β-Ga_2O_3. Therefore, α-Ga_2O_3 has the potential to be used for low-cost fabrication of devices such as high breakdown voltage power devices or solar blind photodetectors (SBPD).

Figure 1a depicts a summary of the representative study fields of α-Ga_2O_3. (i) Bandgap engineering of α-Ga_2O_3, which involves tailoring the bandgap energy of α-Ga_2O_3 by alloy it with other corundum-structured materials such as α-Ti_2O_3 [22–24], α-Rh_2O_3 [25–27], α-Fe_2O_3 [28–32], α-Cr_2O_3 [33–35], α-Ir_2O_3 [36–39], α-In_2O_3 [40–42], and α-Al_2O_3 [43–55], is the first topic. The engineering can be an important technology for fabricating heterojunction devices. Bandgap energies of the alloys based on α-Ga_2O_3 are expected to be tunable from 0.1 to 9.0 eV, while conductivities of the alloys are still being studied, except for Si-doped α-$(Al_xGa_{1-x})_2O_3$ [56]. The second is the techniques for enhancing crystal quality of α-Ga_2O_3, such as (ii) growth on buffer layers, (iii) epitaxial lateral overgrowth (ELO), and (iv) selective area growth (SAG). It was reported that large threading dislocations (TDs) density of ~$10^{10}/cm^2$ exists in α-Ga_2O_3 on sapphire owing to the lattice mismatch and the difference of thermal expansion coefficient between the film and the substrate [57, 58]. The improved crystal quality of α-Ga_2O_3 with the above techniques have been reported. The third topic is (v) the n-type doping with Si [57, 59], and Sn [60–63] for securing the conductivity of α-Ga_2O_3 thin films. Although p-type doping is still a challenge, the possibility of fabricating pn heterojunction with p-type corundum materials such as α-Ir_2O_3 [37–39], and α-Rh_2O_3 [27] can be a unique advantage of the α-phase. The last is the device fabrication based on α-Ga_2O_3 such as (vi) power devices and (vii) SBPDs.

Published papers and citations on α-Ga_2O_3 have increased for the last ten years, as shown in Fig. 1b. Although the percentage of articles for the α-Ga_2O_3 to the β-Ga_2O_3 stays around 20% in 2021, but the fact that the number of publications is gradually increasing shows that researchers become more interested in the α-Ga_2O_3. Furthermore, the research fields have expanded from experimental investigations such as thin film growth and device fabrication process like plasma etching [64] to theoretical calculations on the

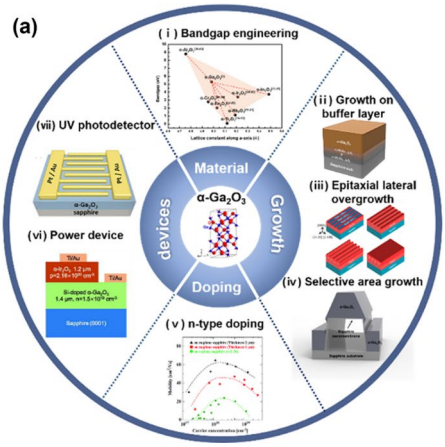

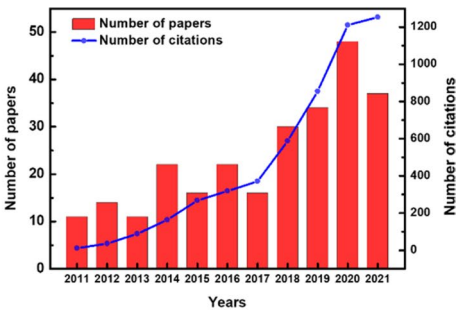

Fig. 1 **a** The outline of research fields on α-Ga_2O_3. **i** Bandgap engineering of α-Ga_2O_3. **ii** α-Ga_2O_3 growth on buffer layers. **iii** Epitaxial lateral overgrowth of α-Ga_2O_3. Reproduced with permission [70]. Copyright 2019, American Chemical Society. **iv** Selective area growth of α-Ga_2O_3. **v** The graph showing mobility as a function of carrier concentration. Reproduced with permission [62]. Copyright 2019, Wiley–VCH. **vi** Schematic of α-Ir_2O_3/α-Ga_2O_3 heterojunction. Reproduced with permission [38]. Copyright 2021, AIP publishing. **vii** Schematic of MSM α-Ga_2O_3 photodetector. Reproduced with permission [114]. Copyright 2021, AVS. **b** The number of publications and citations on α-Ga_2O_3 per year conducted since 2011. The publication search was performed using the web of science [v.5.35]–web of sciencecore collection search: keywords of alpha gallium oxide or (α-Ga_2O_3) have been used

material's properties. So, we want to provide insight into the promising material by summarizing progress on epitaxial growth and doping of α-Ga_2O_3 crystals and their current applications such as electronic and optoelectronic devices in this review.

2 Epitaxial Growth

Various growth techniques for growing single-crystalline α-Ga_2O_3 thin films on sapphire substrates have been used, such as the halide vapor phase epitaxy (HVPE), the mist chemical vapor deposition (mist CVD), the molecular beam epitaxy (MBE), the atomic layer deposition (ALD), the metalorganic chemical vapor deposition (MOCVD), etc. This section will introduce the outcomes of the growth techniques and discuss their benefits and challenges.

2.1 Halide Vapor Phase Epitaxy

HVPE is a CVD technique known for the high purity of resultant thin films with a rapid growth rate. Figure 2a shows the schematic of HVPE for epitaxial growth of α-Ga_2O_3. In HVPE, an α-Ga_2O_3 thin film is synthesized through a series of reactions using carbon-free sources such as Ga metal, hydrochloric acid (HCl), and oxygen gas typically at 450–550 °C [65]:

$$Ga(Liquid) + HCl(Gas) \rightarrow GaCl(Gas) + 1/2H_2(Gas)$$

$$2GaCl(Gas) + 3/2O_2(Gas) \rightarrow Ga_2O_3(Solid) + Cl_2(Gas)$$

resulting in low impurity concentration. The study on epitaxial growth of α-Ga_2O_3 films on c-plane sapphire substrates with HVPE includes the direct growth and the ELO for crystallinity improvement.

2.1.1 Direct Growth

In 2015, Oshima et al. [66] reported the epitaxial growth of twin-free α-Ga_2O_3 films on c-plane sapphire substrates for the first time. They confirmed that the thin films grown by HVPE had much lower impurity concentrations, such as H, C, Si, than those grown by mist CVD, and demonstrated a rapid growth rate as high as approximately 150 μm/h. Leach et al. [67] reported that the surface preparation of the substrate is the key for high-quality and single-crystalline α-Ga_2O_3 thin films. Since 2019, Jeon's group has reported the growth optimization process by adopting the post-growth annealing process and O_2 pulsed mode, as shown in Fig. 2b [57, 65, 68]. They explicated that the annealing could increase the number of Ga-O bonds for the stoichiometric ratio [68], and the O_2 pulsed mode promoted the diffusion length of Ga adatoms longer [57]. In 2020, Lee et al. [69] reported the highly crystalline α-Ga_2O_3 single crystals with the full width at half maximum (FWHM) values of XRD ω-rocking curves for the 0006 and $10\bar{1}2$ reflections of 61 and 1016 arcsec, respectively, on bare sapphire substrates. Despite the low values, however, the TD density taken from plane-view TEM images was still high of low $10^{10}/cm^2$ in

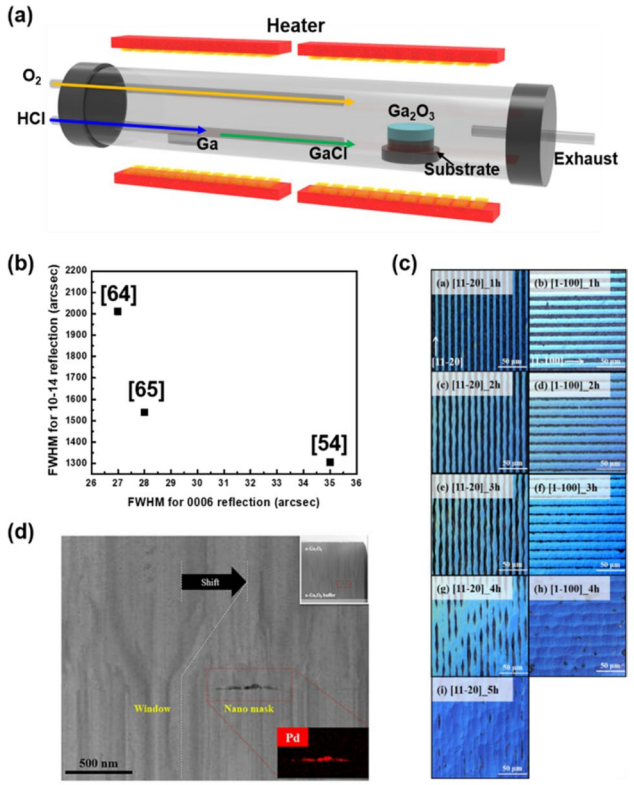

Fig. 2 **a** Schematic of HVPE for epitaxial growth of α-Ga_2O_3. **b** The FWHM values for $10\bar{1}4$ reflections of α-Ga_2O_3 grown by HVPE as a function of the FWHM values for 0006 reflections with optimizing growth conditions. **c** Cross-sectional TEM image of ELO α-Ga_2O_3 on buffer layer with Pd-SWCNTs. Reproduced with permission [71]. Copyright 2019, AIP Publishing. **d** Plane-view optical microscope images of ELO α-Ga_2O_3 on SiN masks along $[11\bar{2}0]$ and $[1\bar{1}00]$ pattern direction depending on the growth time. Reproduced with permission [70]. Copyright 2019, American chemical society

α-Ga_2O_3, which remains still a critical drawback [57, 58, 69].

2.1.2 Epitaxial Lateral Overgrowth

To reduce TD density in an α-Ga_2O_3 film grown on a sapphire substrate, ELO, a technique to block dislocations threading from the substrate or substrate/buffer structure to the next-grown epitaxial layers, has been adopted in HVPE. HVPE is a favorable method to obtain fully coalesced thin films through ELO due to the rapid growth rate. Oshima et al. [58] demonstrated the ELO of α-Ga_2O_3 on stripe patterned SiO_2 masks and achieved a low TD density of less than $5 \times 10^6/cm^2$ in the wing area where the lateral growth was dominant, estimated by plane-view TEM images. Son et al. [70] used SiN masks along the α-Ga_2O_3 $[11\bar{2}0]$ and $[1\bar{1}00]$, claiming that the $[1\bar{1}00]$ direction is suitable for ELO because of the higher lateral growth rate of α-Ga_2O_3, as shown in Fig. 2c. Cha et al. [71] used Pd nanoparticles/single-walled carbon nanotubes (Pd-SWCNTs) for nanomasks for ELO. They reported that high-quality ELO α-Ga_2O_3 on the substrate was achieved, by showing the TD density was $6.10 \times 10^9/cm^2$ evaluated by the cross-sectional TEM images and the FWHMs of XRD ω-scan for the symmetric 0006 and skew-symmetric $10\bar{1}4$ reflections were 17 and 879 arcsec, respectively. Figure 2d reveals that dislocations were bent, which is the main reason for reducing TDs. Son et al. [72] showed crystallinity improvement of α-Ga_2O_3 thin films on conical frustum patterned sapphire substrates also occurred through ELO by revealing an average TD density of $8.4 \times 10^9/cm^2$ from the plane-view TEM images. Kawara et al. [73] studied on the in-plane anisotropy of dislocation bending in ELO α-Ga_2O_3. They observed that TDs in the ELO region were bent toward the $<10\bar{1}0>$ directions by applying the etch-pit method using KOH aqueous solution on the polished ELO epilayer. Furthermore, Kawara et al. [74] demonstrated the double-layered ELO (DLELO) where the ELO was performed twice for eliminating TDs propagating on the area of the first window, and successfully obtained a continuous α-Ga_2O_3 thin film whose thickness was about 100 μm, although the surface was bumpy. They estimated TD density of $5 \times 10^6/cm^2$ with the plane-view TEM images. If the surface roughness is improved, the DLELO process will be helpful for obtaining thick α-Ga_2O_3 films.

As discussed above, the HVPE is an ideal growth technique for enhancing the crystal quality of α-Ga_2O_3 films by ELO due to its rapid growth rate. In addition, the ability to grow the high purity films is a critical advantage of HVPE. As a result, this method is expected to be utilized to produce freestanding α-Ga_2O_3 substrates as in case of SiC [75], AlN [76], or GaN [77]. The fabrication of freestanding α-Ga_2O_3 substrates will be an important technique to realize homoepitaxial growth of α-Ga_2O_3.

2.2 Mist Chemical Vapor Deposition

Mist CVD is atmospheric equipment for growing thin films with simplicity, safety, and low-cost characteristics. In the mist CVD, an aqueous source with precursors is atomized by ultrasonic vibrators, and then the generated mist is transported by carrier and dilution gases to the heated substrate surface, as shown in Fig. 3a. The mist reacts on the substrate, followed by film formation. The CVD was widely used for α-Ga_2O_3 epitaxial growth on sapphire, reporting various results such as the direct growth, the alloying with other corundum materials, the techniques for crystal-quality improvement, and enhanced thermal stability. Recently, the growth mechanism of α-Ga_2O_3 with mist CVD has been also presented.

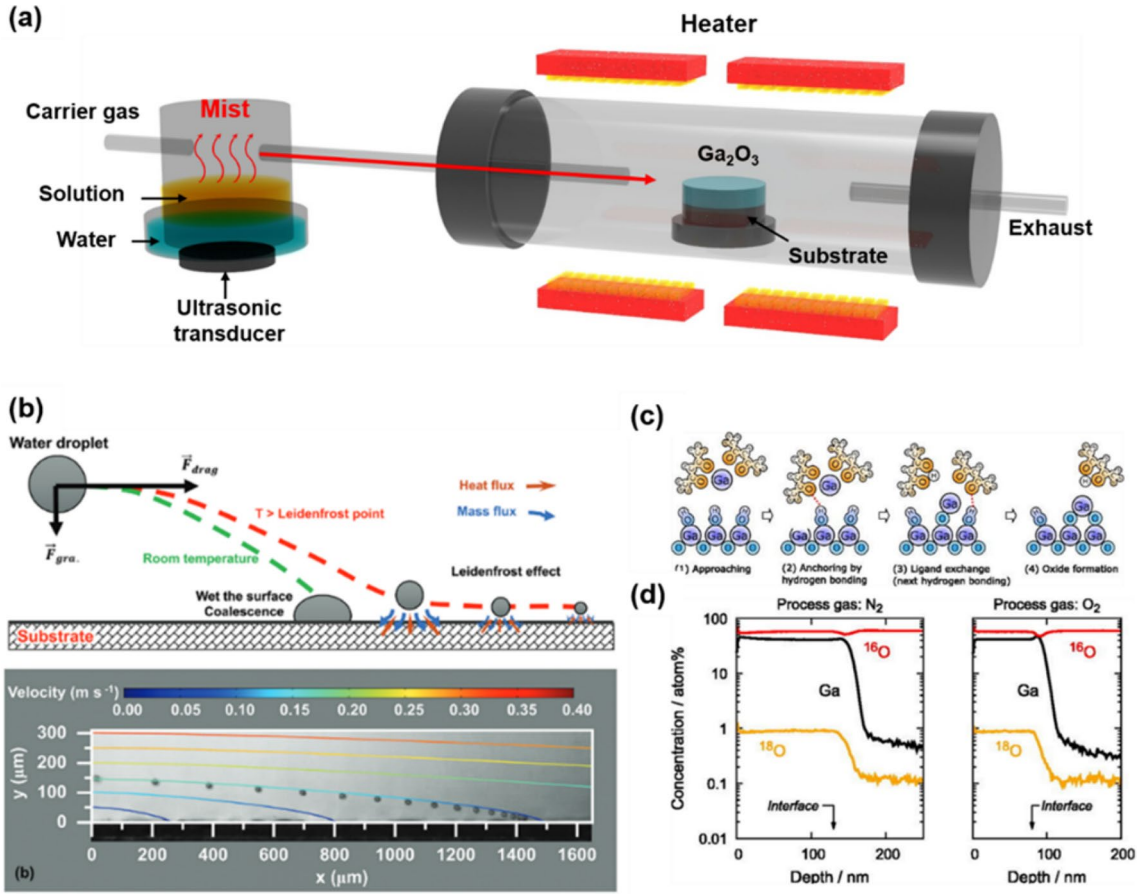

Fig. 3 **a** Schematic of mist CVD fop epitaxial growth of α-Ga_2O_3. **b** Schematic of water droplet motion on substrate surface depending on surface temperature and a high-speed camera image of the water droplet. Reproduced with permission [78]. Copyright 2021, Wiley–VCH. **c** Schematic of the growth mechanism of α-Ga_2O_3 in mist CVD. **d** Concentration profiles of ^{18}O, ^{16}O, and Ga atoms of the α-Ga_2O_3 thin films grown with mist CVD. Reproduced with permission [79]. Copyright 2020, AIP publishing

2.2.1 Growth Mechanism

Recently, studies supporting the Leidenfrost effect as a growth mechanism of mist CVD have been published. The Leidenfrost effect is a physical phenomenon where a liquid forms an insulating vapor layer near a much hotter surface than the liquid's boiling point, preventing the liquid from boiling fast. Ha et al. [78] successfully observed the Leidenfrost motion of water microdroplets on the substrate surface using a high-speed camera, as shown in Fig. 3b. Uno et al. [79] elucidated a growth mechanism by using acetylacetonated Ga solution. Figure 3c shows the reaction process in which acetylacetonate ligands' anchoring follows a ligand exchange by hydrogen bonding. Also, they proved that the oxygen atoms in α-Ga_2O_3 thin films come from water in mist source by examining the $^{18}O/^{16}O$ ratio through secondary ion mass spectroscopy (SIMS), as shown in Fig. 3d.

2.2.2 Direct Growth

In 2008, Shinohara et al. [9] reported the epitaxial growth of α-Ga_2O_3 on sapphire substrates by mist CVD for the first time. Hao et al. [80] demonstrated high uniformity with deviations less than 3% of α-Ga_2O_3 single crystal on 2-inch sapphire. Ma et al. [81, 82] successfully obtained single-crystalline 8-μm-thick-α-Ga_2O_3 films without any crack by the slow cooling rate (< 50 K/h). They also observed the TD behaviors in the α-Ga_2O_3 film through the two-beam bright field TEM images with different diffraction vectors of [0002], $[\bar{2}110]$, and $1/3[\bar{2}116]$, as shown in Fig. 4a–c, respectively [82]. Figure 4a shows that no recognizable pure screw dislocations are observed while Fig. 4b represents pure edge dislocations that can be distinguished. The contrast caused by dislocations in three two-beam images is nearly identical, implying that edge dislocations with the Burgers vector of $b_e = 1/3\langle\bar{2}110\rangle$ have a high density at

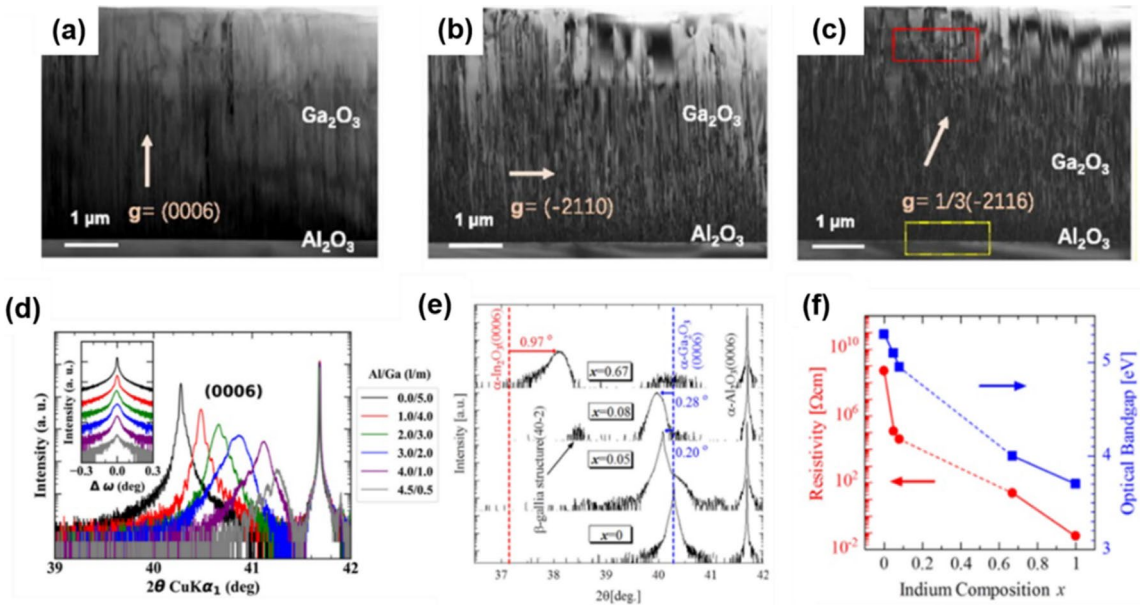

Fig. 4 Cross-sectional TEM images of 8-um-thick α-Ga_2O_3 thin films with different diffraction vectors of **a** [0002], **b** [$\bar{2}$110], and **c** 1/3[$\bar{2}$116]. Reproduced with permission [82]. Copyright 2019, AIP Publishing. **d** XRD theta-2theta scan of α-$(Al_xGa_{1-x})_2O_3$ thin films depending on aluminum contents by mist CVD. Reproduced with permission [49]. Copyright 2018, AIP Publishing. **e** XRD theta-2theta spectra, **f** resistivity and optical bandgap of α-$(In_xGa_{1-x})_2O_3$ thin films as a function of In contents. Reproduced with permission [42]. Copyright 2014, Elsevier B.V

the film-substrate interface and extend along with the film normal.

2.2.3 Alloying

The studies on the alloying α-Ga_2O_3 with other corundum structured oxide materials by mist CVD have been actively underway. Ito et al. [43] successfully demonstrated the epitaxial growth of α-$(Al_xGa_{1-x})_2O_3$ on sapphire by using distilled (DI) water containing both aluminum acetylacetonate ($Al(acac)_3$) and gallium acetylacetonate ($Ga(acac)_3$) as a precursor for the first time in 2012. In 2018, Dang et al. [49] synthesized α-$(Al_xGa_{1-x})_2O_3$ single crystals by introducing a mist CVD two-chamber system to avoid side reactions that occurred when Al and Ga sources were mixed in one chamber, and succeeded in controlling Al contents by simply changing the Al and Ga carrier gas flow rates, as shown in Fig. 4d. In addition, single-crystalline α-$(In_xGa_{1-x})_2O_3$ whose In contents x increased from 0 to 0.67 was demonstrated, as shown in Fig. 4e [42]. Figure 4f shows that the resistivity and the bandgap decreased by increasing In contents [42]. α-$(Ga_{1-x}Fe_x)_2O_3$ [31, 35, 83] and α-$(Ga_{1-x}Cr_x)_2O_3$ [35] have also been demonstrated by mist CVD. Kaneko et al. [31] demonstrated the epitaxial growth of α-$(Ga_{1-x}Fe_x)_2O_3$ thin films with room-temperature magnetism in which there was no phase-separated area confirmed by TEM energy-dispersive X-ray spectroscopy.

2.2.4 Techniques for Crystallinity Improvement

Several trials have enhanced the crystal quality of α-Ga_2O_3 thin films on sapphire substrates such as a buffer layer, ELO on dielectric patterns, and sapphire nanomembrane. Typically, α-$(Al_xGa_{1-x})_2O_3$ layers have been used for an intermediate layer of α-Ga_2O_3 and α-Al_2O_3 for growing thick [46] and high crystalline[48, 84] α-Ga_2O_3. α-Fe_2O_3 was also used as a single [85] and a multiple-quantum-well (MQW) [86] layer for improving the crystallinity of α-Ga_2O_3. Especially, the results of quasi-graded α-$(Al_xGa_{1-x})_2O_3$ layers [48, 87] and the MQW [86], which is shown in Fig. 5a, show the remarkable growth controllability of mist CVD.

ELO was also demonstrated by using SiO_2 [88] and SiO_x [89] masks. Jinno et al. [88] achieved merged thin films on stripe patterned SiO_2 masks using a-plane sapphire substrates where α-Ga_2O_3 can grow in the rectangular facet structures with the largest lateral growth rate. Recently, Dang et al. [89] demonstrated ELO α-Ga_2O_3 on stripe patterned SiO_x masks with under 600 nm pitch on an α-Ga_2O_3 template. Figure 5b is the coalescence α-Ga_2O_3 image with a small thin film thickness on the sub-μm patterns. Lately, Yang et al. [90] reported the selective area growth of high-quality and strain-relaxed α-Ga_2O_3 on sapphire nanomembranes, as shown in Fig. 5c. Stripe-patterned cavity structures provide thin substrates of 60 nm, which reduce the thin films' strain by sharing the total strain energy. They confirmed that the misfit dislocation density in α-Ga_2O_3 on

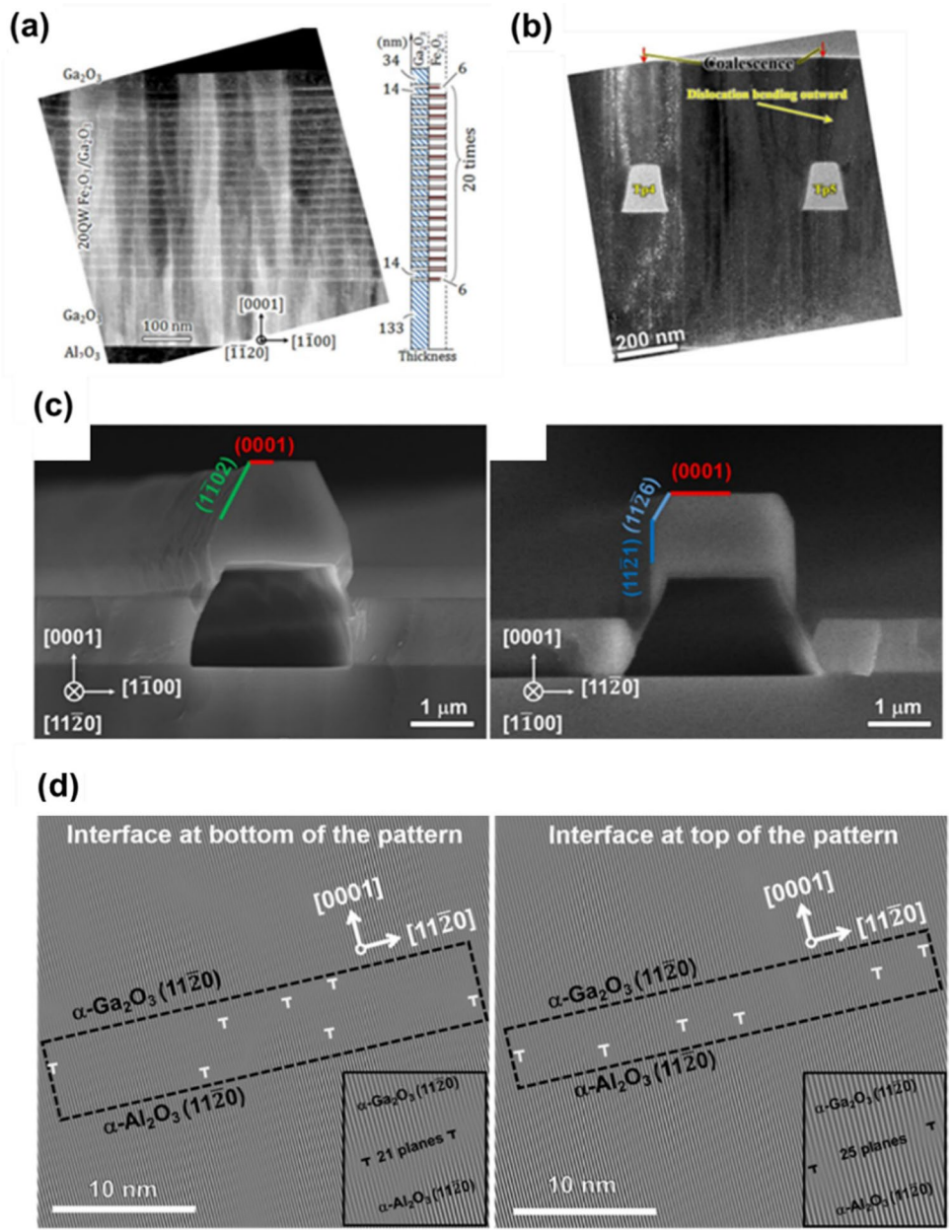

Fig. 5 Various techniques for high-quality α-Ga_2O_3 by mist CVD. TEM images of α-Ga_2O_3 on **a** MQW and **b** SiO_x sub-micrometer patterns. Reproduced with permission [86]. Copyright 2016, AIP Publishing. Reproduced with permission [89]. Copyright 2021, AIP Publishing. **c** SEM images of α-Ga_2O_3 selectively grown on sapphire nanomembrane with the stipe patterns lying in the [11$\bar{2}$0] and [1$\bar{1}$00] directions. **d** Reconstructed TEM images of α-Ga_2O_3 on the bottom and top of the pattern lying in the [1$\bar{1}$00] direction. Reproduced with permission [90]. Copyright 2021, American chemical society

sapphire nanomembrane was reduced by 13% compared with that on the thick substrate by reconstructed TEM images through fast Fourier transformation, as shown in Fig. 5d.

2.2.5 Enhanced Thermal Stability

Due to the metastability of α-Ga_2O_3, at growth temperatures over 550 °C, β-Ga_2O_3 [9] or ε-Ga_2O_3 [87] grow in the α phase dominated films. In addition, when α-Ga_2O_3 was annealed at temperatures over 600 °C, β-Ga_2O_3 started to appear in the film [45, 91]. Since the low thermal stability of α-Ga_2O_3 limits the utilization at high temperature, enhancing the stability is an important issue. Lee et al. [45] were the first to show that adding Al to α-Ga_2O_3 can improve the α-phase's thermal stability. When annealed at temperatures up to 650 °C, the Al doped α-Ga_2O_3 thin film maintained its phase, but the undoped α-Ga_2O_3 thin film started to include β-Ga_2O_3 at temperatures over 600 °C. In addition, α-$(Al_{0.2}Ga_{0.8})_2O_3$ thin films withstand the annealing temperature of 850 °C by retaining the α-phase. In 2020, Jinno et al. [92] reported that inverse relationship between thermal stability and film thickness of α-Ga_2O_3. They also showed that the thermal stability of SAG α-Ga_2O_3 on dot patterned SiO_2 was improved by demonstrating that the phase was retained after annealing at 800 °C for 10 h. They explained that the findings were due to the reduction of thermal stress caused by reducing the film thickness or employing the SAG. Thermal stress regulation might be a fundamental

requirement for thermally stable α-Ga_2O_3 thin films on sapphire substrates.

Mist CVD, as previously noted, has played a significant part in the research of α-Ga_2O_3 by yielding diverse results. The ability to grow high-quality α-Ga_2O_3 thin films and the ease of alloying are powerful characteristics of mist CVD for fabricating α-Ga_2O_3-based devices. Although the low growth rate and purity can be disadvantages, using a chlorine-based source is expected to improve them.

2.3 Molecular-Beam Epitaxy

MBE is a growth technique that is useful for synthesizing high-crystalline thin films with atomically sharp surfaces and managing precise doping profiles in the films. The results of epitaxial growth of α-Ga_2O_3 alloys as well as ternary alloys on sapphire substrates have been reported.

2.3.1 Epitaxial Growth of α-Ga_2O_3

The reports on MBE-grown-α-Ga_2O_3 have been published since 2016 [93–96]. Guo et al. [93] firstly obtained single-crystalline α-Ga_2O_3 on m-plane sapphire substrate by MBE. Oshima et al. [94] fabricated α-Al_2O_3/Ga_2O_3 superlattices with epitaxial structures coherently grown on r-plane sapphire substrates and verified that the critical thickness of α-Ga_2O_3 on α-Al_2O_3 was as small as ~1 nm due to the large lattice mismatch. Cheng et al. [96] investigated critical thickness of an α-Ga_2O_3 layer at which β-Ga_2O_3 formed to be 14.4 nm on a-plane substrates. In 2018, Kracht et al. [95] demonstrated, on a r-plane sapphire substrate, growth of an α-Ga_2O_3 film stabilized up to a thickness of 217 nm, and observed c-plane facets of α-Ga_2O_3 on surface facilitated the formation of β-Ga_2O_3 in MBE growth condition.

2.3.2 Alloying

Studies on alloying α-Ga_2O_3 with α-Al_2O_3 were achieved by MBE. [54, 55, 97] Jinno et al. [54] grew single-crystalline α-$(Al_xGa_{1-x})_2O_3$ layers whose Al composition was from 0 to 1 with MBE. They used m-plane sapphire substrates as templates for epitaxial growth of α-Ga_2O_3 because the substrates are beneficial for growing the alpha phase by suppressing c-plane formation perpendicular to growth front. McCandless et al. [55] grew α-$(Al_xGa_{1-x})_2O_3$ films with the aluminum composition of 0, 46, and 100% on m-plane sapphires, and annealed the samples to explore the thermal stability. They observed that the pristine α-Ga_2O_3 was converted to the β phase upon the post-growth annealing at temperatures above 800 °C, whereas α-$(Al_xGa_{1-x})_2O_3$ samples with Al composition of 46 and 100% were maintained without phase transition up to the temperature 900 °C. In addition, they deposited an Al_2O_3 cap layer on an α-Ga_2O_3, which improved the film thermal stability up to 900 °C by suppressing decomposition of the film and allowing Al to diffuse into the film.

As previously stated, the crystalline orientation of the wafer was critical for growing single-crystalline α-Ga_2O_3 on sapphire using MBE, resulting in r-plane sapphire substrates being appropriate templates. Furthermore, results on alloying α-Ga_2O_3 with other materials or fabricating heterostructures with α-Ga_2O_3 will be expected based on MBE's precise alloying controllability.

2.4 Atomic Layer Deposition

ALD is a deposition technique characterized by its precise thickness controllability, wafer-scale uniformity, and tunable film composition. Most studies have reported the deposition of amorphous Ga_2O_3 films, however, the results of α-Ga_2O_3 have been reported since 2018 [22, 98–103].

Roberts et al. [98] was the first to succeed in growing a Ga_2O_3 thin film with a dominant α phase with some ε and amorphous phases on a c-plane sapphire substrate at 250 °C. The α phase in the film showed an epitaxial relationship with the substrate of $\left[11\bar{2}0\right]_{Ga2O3} \| \left[11\bar{2}0\right]_{Al2O3}$, $(0001)_{Ga2O3} \| (0001)_{Al2O3}$, and a low FWHM of 22 arcsec for 0006 reflection of α-Ga_2O_3 despite the inclusion of other phases. In 2020, Wheeler et al. [101] successfully controlled the phase of Ga_2O_3 by tuning growth conditions such as growth temperature, pressure, and total gas flow, and succeeded in epitaxial growth of an α-Ga_2O_3 film with thickness of 45 nm on a c-plane sapphire substrate at 295 °C under a plasma generated in 40 sccm pure O_2 at low pressures. Moloney et al. [102] found the α-Ga_2O_3 films were stable up to 400 °C during post-growth annealing and confirmed the thermal annealing enhanced the crystalline quality due to the strain relaxation. Finally, Barthel reported the synthesis of α-$(Ti_xGa_{1-x})_2O_3$ spanning x from 0 to 5.3% although degradation of crystalline quality was observed over 3.7%, however, the alloy has a potential for bandgap engineering ranging from 0.1 to 5.3 eV.

As previously mentioned, ALD was used to grow α-Ga_2O_3 films at low temperatures, and single-crystalline α-Ga_2O_3 thin films were successfully demonstrated. ALD-grown α-Ga_2O_3 has a low thermal budget, which might be beneficial for overlayer growth and fabricating cost-effective devices.

2.5 Metalorganic Chemical Vapor Deposition

MOCVD is a thin film growth technique based on a chemical reaction of organometallic and gaseous sources. This method is well-known for the large-scale and fast deposition of nitride and oxide thin films. However, results on

α-Ga_2O_3 by MOCVD have been limited to direct growth on sapphire substrates due to an extremely tight growth window of single-crystalline α-Ga_2O_3. In 2015, Schewski et al. [104] firstly found that α-Ga_2O_3 consisting of only three monolayers epitaxially grown at 850 °C with MOCVD at the interface between c-plane sapphire substrate and the β-Ga_2O_3. Reports on a mixture α- and ε-Ga_2O_3 film with a dominant α phase, not single-crystalline α-Ga_2O_3 with MOCVD by increasing HCl flow have been reported since 2018 [105, 106]. Sun et al. [105] proposed that the HCl acts as a catalyst during the phase transformation in MOCVD. In 2020, Egyenes-Pörsök et al. [107] successfully grew single-crystalline α-Ga_2O_3 thin films on m-plane sapphire substrates at 700 °C using liquid-injection MOCVD under high O_2 flow condition (170 sccm).

Growth window for α-Ga_2O_3 growth on sapphire with MOCVD is narrow. However, as liquid-injection MOCVD succeeded in single-crystalline α-Ga_2O_3 growth, we anticipate being able to enlarge the window adopting various approaches based on experimental and theoretical inquiry.

3 Doping

The n-type conductivity of α-Ga_2O_3 has been controlled by doping with Sn, Si, and F by the mist CVD and the HVPE. Table 1 summarizes electrical properties such as carrier concentration and hall mobility of α-Ga_2O_3 crystal depending on dopants. Also, we will briefly cover the electrical properties of p-type corundum structures such as α-Ru_2O_3 and α-Ir_2O_3, which can form pn heterojunction with n-type α-Ga_2O_3.

In mist CVD, Sn doping was achieved by adding a tin (II) chloride dehydrate in Ga source solution. Akaiwa et al. [61, 62] confirmed that the crystallinity of epilayer is the main factor in obtaining high electron mobility and successfully growing the Sn-doped α-Ga_2O_3 with electron mobility of 24 and 65 cm^2/V s on average c-plane and m-plane sapphire substrate by inserting buffer layer. In HVPE, Polyakov et al. [108] grew Sn-doped α-Ga_2O_3 films on sapphire substrates, which has shallow donor concentration from 1.1×10^{17} to $4.8\times10^{19}/cm^3$.

Si-doped α-Ga_2O_3 epilayers have been grown using $C_6H_{12}ClNSi$ as a Si precursor in mist CVD. Uchida et al. [59] proved thermal annealing deteriorates conductivity of Sn-doped α-Ga_2O_3 due to the bonding change and out-diffusion of Sn via hard X-ray photoelectron spectroscopy and X-ray photoemission spectroscopy. They successfully grew Si-doped α-Ga_2O_3, whose maximum carrier mobility was 31.5 cm^2/V s in mist CVD after thermal annealing, unlike Sn doping. Even conductive Si-doped α-$(Al_xGa_{1-x})_2O_3$ thin films with high thermal resistance were reported [56]. In HVPE, Son et al. [57] obtained Si-doped α-Ga_2O_3 epilayers of the maximum electron mobility value of 51.57 cm^2/V s with carrier concentration of $2\times10^{18}/cm^3$ in O_2 pulsed mode.

Morimoto et al. [109] demonstrated the growth of F-doped α-Ga_2O_3 with a low electrical resistivity of 6.2×10^{-2} Ω cm on sapphire substrates by mist CVD. However, a low activation ratio of 10% remains one of the challenges due to the high impurity level.

Table 1 Summary of properties of α-Ga2O3 depending on dopant materials

Dopant	Dopant source	Ga source	Growth technique	Carrier concentration [cm^{-3}]	Mobility [cm^2/V s]	Thickness [nm]	FWHM [arcsec] 0006	FWHM [arcsec] $10\bar{1}4$	Ref.
Sn	$SnCl_2$ (dihydrate)	Ga (acac)$_3$	Mist CVD	Low 10^{18}	~0.6	~200	70	–	[63]
				7×10^{18}	0.23	~200	64	–	
				~7×10^{16}	~0.6	~275	60	–	
				Low 10^{19}	19	2500	20	1000	[61]
				High 10^{18}	5	600	–	1500	
				High 10^{18}	15	1200	–	1100	
				2×10^{18}	24	1200	–	1000	
				~5×10^{18}	~45	1000	–	1450	[62]
				1.2×10^{18}	65	2000	–	1230	
Si	$C_6H_{12}ClNSi$	Ga (acac)$_3$	Mist CVD	3×10^{18}	31.5	–	–	–	[59]
				2.5×10^{19}	0.7	293	–	–	[56]
	SiH_4	Ga	HVPE	2×10^{18}	20	1080	~28	2011	[57]
				Low 10^{18}	2.5	960	~35	3202	
				2×10^{18}	51.57	1430	~35	1306	
F	NH_4F	$GaCl_3$	Mist CVD	1.3×10^{19}	4.6	1560	~100	–	[109]

Although p-doping has not been achieved in α-Ga_2O_3, the epitaxial growth of p-type corundum-structured α-Rh_2O_3 [26, 27] and α-Ir_2O_3 [38, 39] were reported. Kaneko et al. [26] firstly reported p-type α-Rh_2O_3 with a hole mobility of 4×10^{-5} cm^2/V s in 1992. In 2018, Kaneko et al. [27] fabricated p-type α-Rh_2O_3 thin films on c-plane sapphire substrates with mist CVD, but theirs conductivity was extremely low because the films are semimetals in which electrons and holes coexist. They overcame the issue by alloying α-Ga_2O_3 to reduce the electron concentration in α-Rh_2O_3, and successfully obtained an α-$(Rh_{0.918}Ga_{0.082})_2O_3$ film whose hole density and mobility were $7.6\times10^{17}/cm^3$ and 1.0 cm^2/V s. In addition, Kaneko et al. [39] recently succeeded in obtaining p-type α-$(Ir_{1-x}Ga_x)_2O_3$ films with a hole concentration of 9.9×10^{18} to $8.1\times10^{19}/cm^3$ and a mobility of 0.13–0.92 cm^2/V s.

Recently, Sharma et al. [110] for the first time, reported the fundamental electron transport mechanism in α-Ga_2O_3. They proposed that the polar optical phonon (POP) scattering is the dominant scattering mechanism in α-Ga_2O_3 and estimated the low field isotropic average electron mobility is about 220 cm^2/V s predominantly limited by the POP scattering already at a doping concentration of $1.0\times10^{15}/cm^3$. Therefore, it is necessary to increase the carrier mobility to the desired level by increasing the crystallinity of the α-Ga_2O_3 thin films and optimizing the doping conditions.

4 Device Applications

Based on the various growth and doping techniques for high-quality α-Ga_2O_3, device applications in power devices, solar-blind photodetectors have been reported. The large bandgap energy of α-Ga_2O_3 is essential for the development of power devices used for precisely controlling and converting electrical energy. Typically, these devices have been fabricated in the form of Schottky barrier diode (SBD) [111] and field-effect transistor (FET) [112]. Furthermore, benefiting from a wide bandgap of 5.0–5.3 eV with intrinsic solar-blindness and absorption cut-off wavelength 260–280 nm, α-Ga_2O_3 is suitable for SBPDs whose potential applications contain early missile threat warning, environmental monitoring, and short-range communications [113]. In this section, the current advances of α-Ga_2O_3-based power devices and SBPDs will be reviewed.

4.1 Power Devices

Although notable results have been published on the epitaxial growth of α-Ga_2O_3 thin films on sapphire substrates, there are only a few published results on α-Ga_2O_3 power devices based on used on mist CVD, as shown in Table 2. In 2015, Dang et al. [112] reported the cost-effective α-Ga_2O_3 based metal–semiconductor FET (MESFET), as shown in Fig. 6a. The Sn-doped α-Ga_2O_3 thin films were etched using HCl solution to fabricate the AgO_x Schottky contacts. This MESFET showed that the rectification ratio and the reverse breakdown voltage were 6×10^6 and 19.6 V, respectively, as shown in Fig. 6b and c. For the first time, Oda et al. [111]

Table 2 Summary of α-Ga_2O_3 power devices

Device structure		Growth method	R_{on} [Ω cm^2]	Breakdown voltage [V]	On/off ratio	Ref.
Sn:α-Ga_2O_3 film	Schottky junction (Pt/Ti/Au)	Mist CVD	0.1×10^{-3}	531	–	[111]
	Schottky junction (Pt/Ti/Au)		0.4×10^{-3}	855		
Sn:α-Ga_2O_3 film	MESFET (AgO_x)	Mist CVD	–	19.6	6×10^6	[112]
Sn:α-Ga_2O_3 film	Schottky junction (PtO_x)	Mist CVD	~1×10	~260	5×10^7	[84]
	Schottky junction (AgO_x)		–	~110	2×10^7	
Si:α-Ga_2O_3 film	Schottky junction (AgO_x)	Mist CVD	0.11–0.18	245	–	[56]
	MESFET (AgO_x)		–	–	2×10^5	
α-Ir_2O_3/Sn:α-Ga_2O_3	pn junction	Mist CVD	–	–	–	[38]
α-(Ir, Ga)$_2O_3$/Sn:α-Ga_2O_3	pn junction	Mist CVD	4.3×10^{-3}	~100	5×10^5	[39]

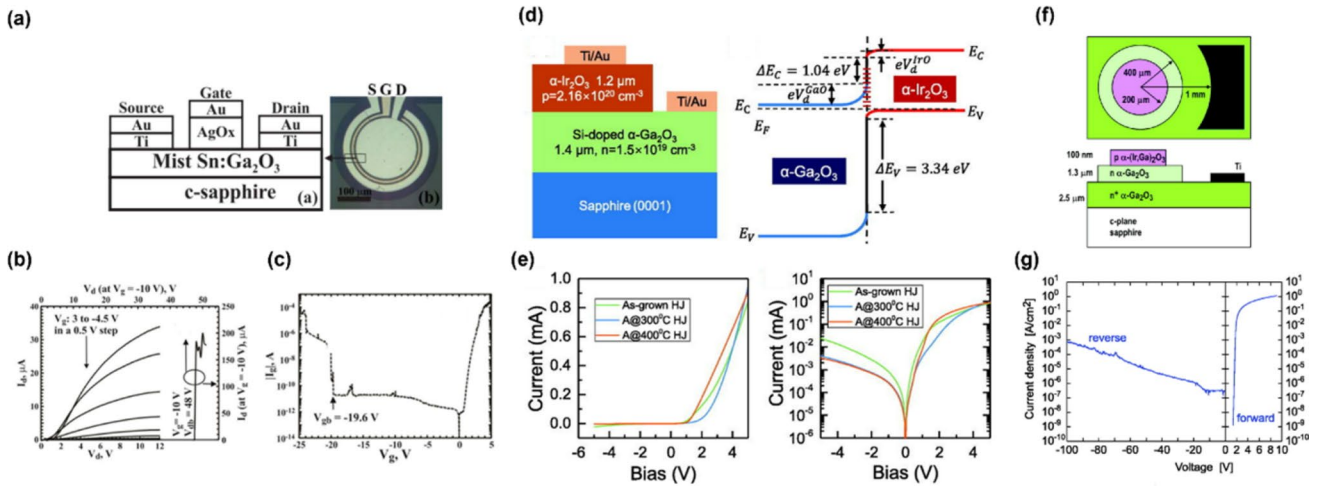

Fig. 6 Device structures and I-V characteristics of α-Ga_2O_3-based power devices. **a** The device structure of AgO_x Schottky contact MESFET corresponding to **b** output characteristics and **c** an I-V curve measured in the extended reverse bias range. Reproduced with permission [112]. Copyright 2015, IEEE. **d** The device schematic, band structure, and **e** I-V characteristics pn heterojunction with α-Ir_2O_3/α-Ga_2O_3. Reproduced with permission [38]. Copyright 2021, AIP Publishing. **f** The device structure of Mg-doped α-$(Ir, Ga)_2O_3$/α-Ga_2O_3 pn heterostructure diodes and corresponding **g** I-V characteristics. Reproduced with permission [39]. Copyright 2021, AIP Publishing

in FLOSFIA reported that they fabricated vertical SBDs with α-Ga_2O_3 films lifted off of the sapphire substrates, and that the transferred film helped reduce series resistance and transfer heat to the mounted heat sink. The SBDs showed low on-resistance and high breakdown voltage of 0.1 mΩ cm^2 and 531 V (SBD1) or 0.4 mΩ cm^2 and 855 V (SBD2), respectively.

As other trials on the fabrication of power devices with α-Ga_2O_3, researchers reported pn heterojunction with corundum-structured p-type oxides such as α-Rh_2O_3 [27] or α-Ir_2O_3 [37–39] epitaxially grown on n-type α-Ga_2O_3. In 2018, Kan et al. [37] reported the band alignment of α-Ir_2O_3/α-Ga_2O_3 pn heterojunction at first. The current–voltage (I-V) characteristics and the band alignment at the α-Ir_2O_3/α-Ga_2O_3 showed the turn-on voltage of 2.0 V and the total barrier height for electrons of 2.4 eV. Hao et al. [38] demonstrated the epitaxy of lattice-matched α-Ir_2O_3/α-Ga_2O_3 pn heterojunction, as shown in Fig. 6d. From the energy band diagram of α-Ir_2O_3/α-Ga_2O_3 heterojunction and the I-V characteristics, the dominant electron transport mechanism was identified to space-charge-limited current conduction. They also found the thermal treatment in oxygen ambient resulted in the reduced reverse leakage current due to the suppression of interfacial traps and activation of acceptors, as shown in Fig. 6e. Recently, Kaneko et al. [39] thought α-Ir_2O_3 was not suitable for fabricating heterojunction devices by forming pn junction with α-Ga_2O_3 due to its relatively narrow bandgap of 3.0 eV and proposed α-$(Ir_xGa_{1-x})_2O_3$ ternary alloy for higher bandgap energy. Figure 6f shows an α-$(Ir_{0.4}Ga_{0.6})_2O_3$/α-Ga_2O_3 pn heterojunction with the reduced lattice mismatch of 0.12% at interface and corresponding bandgap energy of about 4 eV. The device exhibited that the catastrophic breakdown did not occur until 100 V, but the reverse current gradually rose with increasing bias, and had the current on/off ratio of 5×10^5, as shown in Fig. 6g.

However, despite α-Ga_2O_3's great potential, there are obstacles such as low thermal conductivity of α-Ga_2O_3 to developing high-performance devices. For reliable operation of α-Ga_2O_3 devices in high voltage, it is necessary to replace sapphire substrates with high thermal conductivity substrates, such as SiC or diamond. Kaneko et al. [27] demonstrated the ability to lifted off the α-Ga_2O_3 films due to the interfacial misfit dislocations and accumulated strain, and successfully fabricated an α-Ga_2O_3 SBD mounted on the TO220 package, exhibiting small thermal resistance of 13.9 °C/W. Recently, Yang et al. [90] demonstrated the SAG α-Ga_2O_3 on thin sapphire nanomembrane, which expects a mechanical lift-off of α-Ga_2O_3 films by breaking the sidewalls to be realized. The transfer results, on the other hand, have yet to be published. Lift-off technologies, which are anticipated to improve heat dissipation by transferring onto other substrates, will become a key for fabricating high-performance α-Ga_2O_3-based devices.

4.2 Solar-Blind Photodetectors

The structure of α-Ga_2O_3 SBPDs usually reported in the literature is the metal–semiconductor-metal (MSM) structure based on the interdigitated electrode, which has advantages of the large photosensitive area, low response time, and

simple fabrication process. Unlike power devices, SBPDs have been fabricated with various growth methods, as shown in Table 3. Guo et al. [93] reported the SBPD based on a 100-nm-thick single-crystalline α-Ga_2O_3 on an m-plane sapphire substrate using laser-MBE. However, the ultraviolet (UV) responsivity was as low as 3–15 mA/W. Lee et al. [69] reported that performance of device fabricated with a high-quality α-Ga_2O_3 film on a c-plane sapphire by HVPE showed the photo-responsivity of 0.19 A/W and detectivity of 4.19×10^{11} Jones, and the rise and fall response time were evaluated be 23 and 204 μsec, respectively. This outstanding fast response time was attributed to electron–hole separation without trapping in defect levels and sufficient carrier lifetime due to the high crystalline-quality of α-Ga_2O_3. Figure 7a shows the schematic of MSM type α-Ga_2O_3 SBPDs using ALD [103]. The device showed a high detectivity with deep UV range and the maximized responsivity of 0.76 A/W at λ = 253 nm, as shown in Fig. 7b. The low dark current and the signal-to-noise ratio were also estimated to be 0.5 pA at 10 V, and 104, respectively.

For improving the SBPD performance, Qiao et al. [113] used the Al nanoparticles (NPs) with surface plasmon effect to enhance light absorption and scattering, as shown in Fig. 7c. The SBPDs fabricated with Al NP decorated α-Ga_2O_3 thin films grown by mist CVD showed the enhanced responsivity of 3.36 A/W at λ = 244 nm, and suppressed the surface leakage currents, compared with those without Al NP exceeding an order of magnitude, as shown in Fig. 7d and e. As another way, Bae et al. [114] demonstrated Si-doped-α-Ga_2O_3-based MSM-typed SBPDs using HVPE, as shown in Fig. 7f. Based on the high crystallinity Si-doped-α-Ga_2O_3 epitaxial thin film with the FWHM for

Table 3 Summary of α-Ga_2O_3 photodetectors

Photodetector	Growth method	R [A/W]	D* [Jones]	EQE [%]	Response time		Ref.
					Rise [τ]	Decay [τ]	
α-Ga_2O_3 film	ALD + Annealing (Ar)	1.17 @ 10 V; 240 nm	–	–	–	–	[102]
α-Ga_2O_3 film	ALD	0.76 @ 10 V; 253 nm	–	–	539 ns	–	[103]
α-Ga_2O_3 film	HVPE	0.19 @ 30 V	4.19×10^{11}	–	23 μs	204 μs	[69]
Si:α-Ga_2O_3 film	HVPE	4.24×10^4 @ 5 V; 254 nm	1.77×10^{11}	2.07×10^5	–	–	[114]
Al NPs decorated α-Ga_2O_3 film	Mist CVD	3.36 @ 5 V; 244 nm	–	656	–		[113]

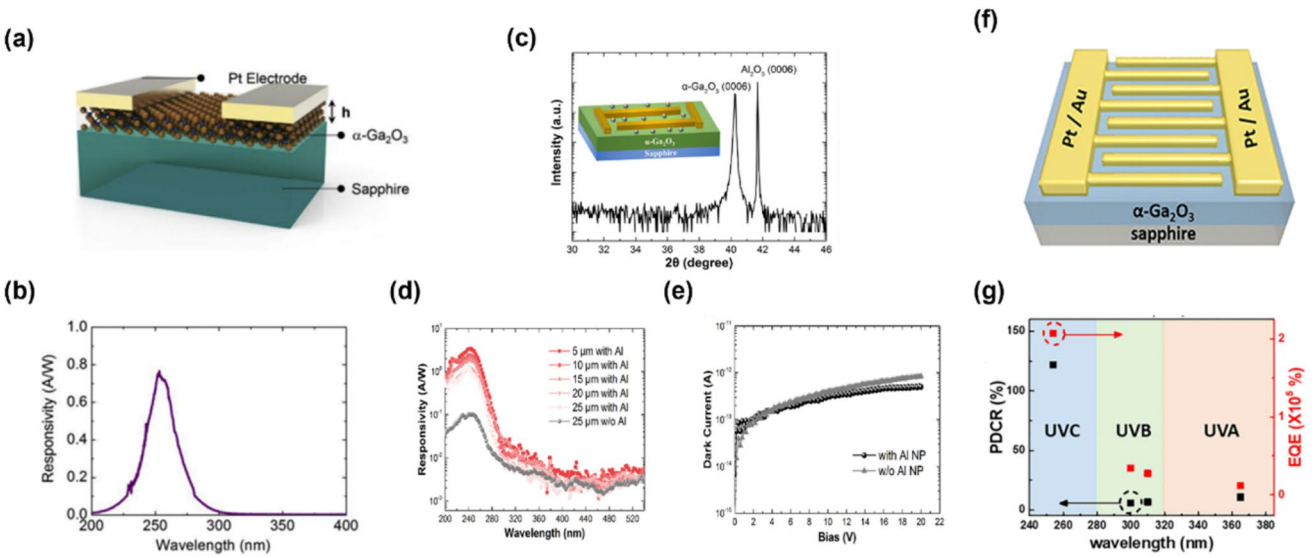

Fig. 7 Device structures and performance of α-Ga_2O_3 MSM SBPDs. **a** Device schematic based on α-Ga_2O_3 grown with low-temperature ALD, **b** Spectral responsivity as a function of wavelengths. Reproduced with permission [103]. Copyright 2018, Elsevier B.V. **c** Device structure and XRD theta/2theta spectrum of Al NPs decorated α-Ga_2O_3 grown by mist CVD, **d** Spectral responsivity of the Al NP-enhanced photodetectors, and **e** the comparison of dark current characteristics of devices with and without Al NPs. Reproduced with permission [113]. Copyright 2019, American chemical society. **f** MSM detector based on Si-doped α-Ga_2O_3 grown by HVPE, **g** photo-to-dark current ratio and EQE (%) under UV regime at 5 V. Reproduced with permission [114]. Copyright 2021, AVS

0006 reflection of 79.8 arcsec, the device showed the high responsivity of 4.24×10^4 A/W with reasonable values of detectivity (1.77×10^{11} Jones) and external quantum efficiency (EQE) (2.07×10^5) under UVC region, as shown in Fig. 7g.

Although enhancing the α-Ga_2O_3's crystallinity is required to improve photo-responsivity, there is also the option of controlling the incident light path. Fresnel reflection, which happens when a refractive index contrast exists between the ambient medium (air) and the photodetector (semiconductor), is a phenomenon that degraded the overall conversion efficiency of the photodetector. Anti-reflection (AR) coatings can be a breakthrough for improving performance by lowering or eliminating Fresnel reflection losses and increasing the amount of light entering the device. For candidate materials for UV-AR coating, fluorides such as MgF_2, AlF_3, LaF_3, and oxides such as HfO_2, Al_2O_3, SiO_2, and UV fused silica are suitable [115]. Single or multi-layer thin film or even nanostructures can efficiently increase the amount of light entering the SBPD. Therefore, results for high-performance SBPDs incorporating the AR technology are expected.

5 Conclusion and Perspective

This review covers the progress on growth and devices of α-Ga_2O_3. In HVPE, high-purity and high-quality α-Ga_2O_3 thin films were demonstrated via ELO process. The HVPE is expected to realize freestanding α-Ga_2O_3 wafers like AlN [76] and GaN [77]. The mist CVD in α-Ga_2O_3 research fields is characterized by easy alloying of α-Ga_2O_3 with various materials, high-quality epitaxial growth based on various techniques. Also, the possibility of growing p-type corundum structured materials increases the value of mist CVD. Studies on growth and doping of α-Ga_2O_3 with various growth methods will enrich the database of α-Ga_2O_3, which is fundamental to the development of the devices.

Though a few results on fabricating power devices exist, the assorted devices were covered, such as the MESFET, the vertical SBDs, and the heterojunction diodes with p-type materials. The increase of thin film quality and doping control abilities based on improved growth technologies is predicted to result in an α-Ga_2O_3-based power device with a high breakdown voltage. In SBPDs, improvement of responsivity for weak solar-blind signals has been achieved by using Al nanoparticles with surface plasmon effects and doping engineering. The evolving technologies will achieve further advances the performance regarding all parameter such as higher responsivity, detectivity, and response time, rather than focusing on specific one116.

Acknowledgements D. Yang, B. Kim, and T. H. Eom contributed equally to this work. This research was supported by the Strategic Core Material Development Program through the Korea Evaluation Institute of Industrial Technology (KEIT) funded by the Ministry of Trade, Industry, and Energy (MOTIE) (No.10080736). The Inter-University Semiconductor Research Center and Institute of Engineering Research at Seoul National University provided research facilities for this work.

Author Contributions D. Yang, B. Kim, T. H. Eom, Y. J. Park, and H. W. Jang conceived of the outline of the manuscript. D. Yang, B. Kim, T. H. Eom wrote the manuscript.

Declarations

Conflict of interest The authors declare no conflict of interest.

References

1. Reese, S.B., Remo, T., Green, J., Zakutayev, A.: How much will gallium oxide power electronics cost? Joule **3**, 903–907 (2019)
2. Yoon, D.-H., Reimanis, I.E.: A review on the joining of SiC for high-temperature applications. J. Korean Ceram. Soc. **57**, 246–270 (2020)
3. Ha, M. T., Shin, Y. J., Bae, S. Y., Park, S. Y., Jeong, S. M. Effect of hot-zone aperture on the growth behavior of SiC single crystal produced via top-seeded solution growth method. J. Korean Ceram. Soc. 56, 589–595 (2019)
4. Jones, E.A., Wang, F.F., Costinett, D.: Review of commercial GaN power devices and GaN-based converter design challenges. IEEE J. Emerg. Selected Top. Pow. Electron. **4**, 707–719 (2016)
5. Shah, F.M., Maqsood, S., Damaševičius, R., Blažauskas, T.: Disturbance rejection and control design of MVDC converter with evaluation of power loss and efficiency comparison of SiC and Si based power devices. Electronics **9**, 1878 (2020)
6. Higashiwaki, M., Murakami, H., Kumagai, Y., Kuramata, A.: Current status of Ga_2O_3 power devices. Jpn. J. Appl. Phys. **55**, 1202A1 (2016)
7. Higashiwaki, M.: β-gallium oxide devices: progress and outlook. Phys. Status Solidi (RRL)–Rapid Res. Lett. **15**, 2100357 (2021)
8. Sasaki, K., Kuramata, A., Masui, T., Villora, E.G., Shimamura, K., Yamakoshi, S.: Device-quality β-Ga_2O_3 epitaxial films fabricated by ozone molecular beam epitaxy. Appl. Phys. Express **5**, 035502 (2012)
9. Shinohara, D., Fujita, S.: Heteroepitaxy of corundum-structured α-Ga_2O_3 thin films on α-Al_2O_3 substrates by ultrasonic mist chemical vapor deposition. Jpn. J. Appl. Phys. **47**, 7311–7313 (2008)
10. Liu, X., Liu, Q., Zhao, B., Ren, Y., Tao, B., Zhang, W.: Comparison of β-Ga_2O_3 thin films grown on r-plane and c-plane sapphire substrates. Vacuum **178**, 109435 (2020)
11. Byun, D. W., Lee, Y. J., Oh, J. M., Schweitz, M. A., Koo, S. M.: Morphological and electrical properties of β-Ga2O3/4H-SiC heterojunction diodes. Electron. Mater. Lett. **17**, 479–484 (2021)
12. Hayashi, H., Huang, R., Oba, F., Hirayama, T., Tanaka, I.: Epitaxial growth of Mn-doped γ-Ga_2O_3 on spinel substrate. J. Mater. Res. **26**, 578–583 (2011)
13. Zhuo, Y., Chen, Z., Tu, W., Ma, X., Pei, Y., Wang, G.: β-Ga_2O_3 versus ε-Ga_2O_3: control of the crystal phase composition of gallium oxide thin film prepared by metal-organic chemical vapor deposition. Appl. Surf. Sci. **420**, 802–807 (2017)
14. Cora, I., Mezzadri, F., Boschi, F., Bosi, M., Čaplovičová, M., Calestani, G., et al.: The real structure of ε-Ga_2O_3 and its relation to κ-phase. CrystEngComm **19**, 1509–1516 (2017)

15. Roy, R., Hill, V., Osborn, E.: Polymorphism of Ga2O3 and the system Ga_2O_3—H_2O. J. Am. Chem. Soc. **74**, 719–722 (1952)
16. Tomm, Y., Ko, J., Yoshikawa, A., Fukuda, T.: Floating zone growth of β-Ga_2O_3: a new window material for optoelectronic device applications. Sol. Energy Mater. Sol. Cells **66**, 369–374 (2001)
17. Kuramata, A., Koshi, K., Watanabe, S., Yamaoka, Y., Masui, T., Yamakoshi, S.: High-quality β-Ga_2O_3 single crystals grown by edge-defined film-fed growth. Jpn. J. Appl. Phys. **55**, 1202a2 (2016)
18. Galazka, Z., Uecker, R., Irmscher, K., Albrecht, M., Klimm, D., Pietsch, M., et al.: Czochralski growth and characterization of β-Ga_2O_3 single crystals. Cryst. Res. Technol. **45**, 1229–1236 (2010)
19. Kasu, M., Hanada, K., Moribayashi, T., Hashiguchi, A., Oshima, T., Oishi, T., et al.: Relationship between crystal defects and leakage current in β-Ga_2O_3 Schottky barrier diodes. Jpn. J. Appl. Phys. **55**, 1202bb (2016)
20. Seiler, W., Selmane, M., Abdelouhadi, K., Perrière, J.: Epitaxial growth of gallium oxide films on c-cut sapphire substrate. Thin Solid Films **589**, 556–562 (2015)
21. Rafique, S., Han, L., Neal, A.T., Mou, S., Boeckl, J., Zhao, H.: Towards high-mobility heteroepitaxial β-Ga2O3 on sapphire–dependence on the substrate off-axis angle. Phys. Status Solidi (A) **215**, 1700467 (2018)
22. Barthel, A., Roberts, J., Napari, M., Frentrup, M., Huq, T., Kovacs, A., et al.: Ti alloyed alpha-Ga_2O_3: route towards wide band gap engineering. Micromachines (Basel) **11**, 1128 (2020)
23. Li, Y., Weng, Y., Yin, X., Yu, X., Kumar, S.R.S., Wehbe, N., et al.: Orthorhombic Ti_2O_3: a polymorph-dependent narrow-bandgap ferromagnetic oxide. Adv. Func. Mater. **28**, 1705657 (2018)
24. Yoshimatsu, K., Hasegawa, N., Nambu, Y., Ishii, Y., Wakabayashi, Y., Kumigashira, H.: Metallic ground states of undoped Ti_2O_3 films induced by elongated c-axis lattice constant. Sci. Rep. **10**, 22109 (2020)
25. Scherson, Y.D., Aboud, S.J., Wilcox, J., Cantwell, B.J.: Surface structure and reactivity of rhodium oxide. J. Phys. Chem. C **115**, 11036–11044 (2011)
26. Koffyberg, F.: Optical bandgaps and electron affinities of semiconducting Rh_2O_3 (I) and Rh_2O_3 (III). J. Phys. Chem. Solids **53**, 1285–1288 (1992)
27. Kaneko, K., Fujita, S., Hitora, T.: A power device material of corundum-structured α-Ga_2O_3fabricated by MIST EPITAXY®technique. Jpn. J. Appl. Phys. **57**, 02cb18 (2018)
28. Zhang, F., Li, X., Zhao, Q., Zhang, Q., Tadé, M., Liu, S.: Fabrication of α-Fe_2O_3/In_2O_3 composite hollow microspheres: a novel hybrid photocatalyst for toluene degradation under visible light. J. Colloid Interf. Sci. **457**, 18–26 (2015)
29. Kraushofer, F., Jakub, Z., Bichler, M., Hulva, J., Drmota, P., Weinold, M., et al.: Atomic-scale structure of the hematite alpha-Fe_2O_3(1102) "R-cut" surface. J. Phys. Chem. C Nanomater. Interf. **122**, 1657–1669 (2018)
30. Kaneko, K., Akaiwa, K., Fujita, S.: Crystal structure of non-doped and Sn-doped α-(GaFe) $_2O_3$ thin films. MRS Online Proc. Library (OPL) **1494**, 147–152 (2013)
31. Kaneko, K., Kakeya, I., Komori, S., Fujita, S.: Band gap and function engineering for novel functional alloy semiconductors: bloomed as magnetic properties at room temperature with α-$(GaFe)_2O_3$. J. Appl. Phys. **113**, 233901 (2013)
32. Zhang, H., Li, L., Liu, C., Wang, W., Liang, P., Mitsuzak, N., Chen, Z.: Carbon coated α-Fe2O3 photoanode synthesized by a facile anodic electrodeposition for highly efficient water oxidation. Electron. Mater. Lett. **14**, 348–356 (2018)
33. Cheng, R., Xu, B., Borca, C.N., Sokolov, A., Yang, C.S., Yuan, L., et al.: Characterization of the native Cr_2O_3 oxide surface of CrO_2. Appl. Phys. Lett. **79**, 3122–3124 (2001)
34. Gibot, P., Vidal, L.: Original synthesis of chromium (III) oxide nanoparticles. J. Eur. Ceram. Soc. **30**, 911–915 (2010)
35. Kaneko, K., Nomura, T., Fujita, S.: Corundum-structured α-phase Ga_2O_3-Cr_2O_3-Fe_2O_3 alloy system for novel functions. Phys. Status Solidi (C) **7**, 2467–2470 (2010)
36. Chesnokov, A., Gryaznov, D., Skorodumova, N.V., Kotomin, E.A., Zitolo, A., Zubkins, M., et al.: The local atomic structure and thermoelectric properties of Ir-doped ZnO: hybrid DFT calculations and XAS experiments. J. Mater. Chem. C **9**, 4948–4960 (2021)
37. Kan, S.-I., Takemoto, S., Kaneko, K., Takahashi, I., Sugimoto, M., Shinohe, T., et al.: Electrical properties of α-Ir_2O_3/α-Ga_2O_3 pn heterojunction diode and band alignment of the heterostructure. Appl. Phys. Lett. **113**, 212104 (2018)
38. Hao, J.G., Gong, H.H., Chen, X.H., Xu, Y., Ren, F.F., Gu, S.L., et al.: In situ heteroepitaxial construction and transport properties of lattice-matched α-Ir_2O_3/α-Ga_2O_3 p-n heterojunction. Appl. Phys. Lett. **118**, 261601 (2021)
39. Kaneko, K., Masuda, Y., Kan, S.-I., Takahashi, I., Kato, Y., Shinohe, T., et al.: Ultra-wide bandgap corundum-structured p-type α-(Ir, Ga)2O3 alloys for α-Ga2O3 electronics. Appl. Phys. Lett. **118**, 102104 (2021)
40. Weiher, R.L., Ley, R.P.: Optical properties of indium oxide. J. Appl. Phys. **37**, 299–302 (1966)
41. García-Domene, B., Sans, J.A., Manjón, F.J., Ovsyannikov, S.V., Dubrovinsky, L.S., Martinez-Garcia, D., et al.: Synthesis and high-pressure study of corundum-type In_2O_3. J. Phys. Chem. C **119**, 29076–29087 (2015)
42. Suzuki, N., Kaneko, K., Fujita, S.: Growth of corundum-structured $(In_xGa_{1-x})_2O_3$ alloy thin films on sapphire substrates with buffer layers. J. Cryst. Growth **401**, 670–672 (2014)
43. Ito, H., Kaneko, K., Fujita, S.: Growth and band gap control of corundum-structured α-$(AlGa)_2O_3$ thin films on sapphire by spray-assisted mist chemical vapor deposition. Jpn. J. Appl. Phys. **51**, 100207 (2012)
44. Santos, R.C.R., Longhinotti, E., Freire, V.N., Reimberg, R.B., Caetano, E.W.S.: Elucidating the high-k insulator α-Al_2O_3 direct/indirect energy band gap type through density functional theory computations. Chem. Phys. Lett. **637**, 172–176 (2015)
45. Lee, S.-D., Ito, Y., Kaneko, K., Fujita, S.: Enhanced thermal stability of alpha gallium oxide films supported by aluminum doping. Jpn. J. Appl. Phys. **54**, 030301 (2015)
46. Oda, M., Kaneko, K., Fujita, S., Hitora, T.: Crack-free thick (~5 μm) α-Ga2O3 films on sapphire substrates with α-(Al, Ga)2O3 buffer layers. Jpn. J. Appl. Phys. **55**, 1202b4 (2016)
47. Kaneko, K., Suzuki, K., Ito, Y., Fujita, S.: Growth characteristics of corundum-structured α-$(Al_xGa_{1-x})_2O_3$/Ga_2O_3 heterostructures on sapphire substrates. J. Cryst. Growth **436**, 150–154 (2016)
48. Jinno, R., Uchida, T., Kaneko, K., Fujita, S.: Reduction in edge dislocation density in corundum-structured α-Ga2O3 layers on sapphire substrates with quasi-graded α-(Al, Ga)2O3 buffer layers. Appl. Phys. Express **9**, 071101 (2016)
49. Dang, G.T., Yasuoka, T., Tagashira, Y., Tadokoro, T., Theiss, W., Kawaharamura, T.: Bandgap engineering of α-$(Al_xGa_{1-x})_2O_3$ by a mist chemical vapor deposition two-chamber system and verification of Vegard's law. Appl. Phys. Lett. **113**, 062102 (2018)
50. Jinno, R., Uchida, T., Kaneko, K., Fujita, S.: Control of crystal structure of Ga_2O_3 on sapphire substrate by introduction of α-$(Al_xGa_{1-x})_2O_3$ buffer layer. Phys. Status Solidi (B) **255**, 1700326 (2018)
51. Uchida, T., Jinno, R., Takemoto, S., Kaneko, K., Fujita, S.: Evaluation of band alignment of α-Ga_2O_3/α-$(Al_xGa_{1-x})_2O_3$

heterostructures by X-ray photoelectron spectroscopy. Jpn. J. Appl. Phys. **57**, 040314 (2018)
52. Chang, C., Jinno, R., Jena, D., Xing, H., Muller, D.: Direct imaging on strain relaxation of MBE-grown single phase alpha-(Al, Ga)$_2$O$_3$ on m-sapphire substrate in atomic resolution using scanning transmission electron microscopy. Bull. Am. Phys. Soc. **65**, 1 (2020)
53. Chen, Z., Arita, M., Saito, K., Tanaka, T., Guo, Q.: Epitaxial growth of $(Al_xGa_{1-x})_2O_3$ thin films on sapphire substrates by plasma assisted pulsed laser deposition. AIP Adv. **11**, 035319 (2021)
54. Jinno, R., Chang, C.S., Onuma, T., Cho, Y., Ho, S.-T., Rowe, D., et al.: Crystal orientation dictated epitaxy of ultrawide-bandgap 5.4-to 8.6-eV α-(AlGa)2O3 on m-plane sapphire. Sci. Adv. **7**, eabd5891 (2021)
55. McCandless, J.P., Chang, C.S., Nomoto, K., Casamento, J., Protasenko, V., Vogt, P., et al.: Thermal stability of epitaxial α-Ga2O3 and (Al, Ga)2O3 layers on m-plane sapphire. Appl. Phys. Lett. **119**, 062102 (2021)
56. Dang, G.T., Tagashira, Y., Yasuoka, T., Liu, L., Kawaharamura, T.: Conductive Si-doped α-(AlxGa1−x)2O3 thin films with the bandgaps up to 6.22 eV. AIP Adv. **10**, 115019 (2020)
57. Son, H., Choi, Y.-J., Park, J.-H., Ryu, B., Jeon, D.-W.: Correlation of pulsed gas flow on Si-doped α-Ga_2O_3 epilayer grown by halide vapor phase epitaxy. ECS J. Solid State Sci. Technol. **9**, 055005 (2020)
58. Oshima, Y., Kawara, K., Shinohe, T., Hitora, T., Kasu, M., Fujita, S.: Epitaxial lateral overgrowth of α-Ga_2O_3 by halide vapor phase epitaxy. APL Mater. **7**, 022503 (2019)
59. Uchida, T., Kaneko, K., Fujita, S.: Electrical characterization of Si-doped n-type α-Ga_2O_3 on sapphire substrates. MRS Adv. **3**, 171–177 (2018)
60. Akaiwa, K., Fujita, S.: Electrical conductive corundum-structured α-Ga_2O_3 thin films on sapphire with tin-doping grown by spray-assisted mist chemical vapor deposition. Jpn. J. Appl. Phys. **51**, 070203 (2012)
61. Akaiwa, K., Kaneko, K., Ichino, K., Fujita, S.: Conductivity control of Sn-doped α-Ga_2O_3 thin films grown on sapphire substrates. Jpn. J. Appl. Phys. **55**, 1202ba (2016)
62. Akaiwa, K., Ota, K., Sekiyama, T., Abe, T., Shinohe, T., Ichino, K.: Electrical properties of Sn-doped α-Ga2O3 films on m-plane sapphire substrates grown by mist chemical vapor deposition. Phys. Status Solidi (A) **217**, 1100632 (2020)
63. Kawaharamura, T., Dang, G.T., Furuta, M.: Successful growth of conductive highly crystalline Sn-doped α-Ga_2O_3 thin films by fine-channel mist chemical vapor deposition. Jpn. J. Appl. Phys. **51**, 040207 (2012)
64. Um, J.H., Choi, B.S., Jeong, D.H., Choi, H.-U., Hwang, S., Jeon, D.-W., et al.: Chlorine-based high density plasma etching of α-Ga_2O_3 epitaxy layer. Electron. Mater. Lett. **17**, 142–147 (2021)
65. Son, H., Jeon, D.-W.: Optimization of the growth temperature of α-Ga_2O_3 epilayers grown by halide vapor phase epitaxy. J. Alloy. Compd. **773**, 631–635 (2019)
66. Oshima, Y., Víllora, E.G., Shimamura, K.: Halide vapor phase epitaxy of twin-free α-Ga_2O_3 on sapphire (0001) substrates. Appl. Phys. Express **8**, 055501 (2015)
67. Leach, J.H., Udwary, K., Rumsey, J., Dodson, G., Splawn, H., Evans, K.R.: Halide vapor phase epitaxial growth of β-Ga_2O_3 and α-Ga_2O_3 films. APL Mater. **7**, 022504 (2019)
68. Son, H., Choi, Y.-J., Hwang, J., Jeon, D.-W.: Influence of post-annealing on properties of α-Ga_2O_3 epilayer grown by halide vapor phase epitaxy. ECS J. Solid State Sci. Technol. **8**, Q3024–Q3027 (2019)
69. Lee, M., Yang, M., Lee, H.-Y., Lee, H.U., Lee, H., Son, H., et al.: The growth of HVPE α-Ga_2O_3 crystals and its solar-blind UV photodetector applications. Mater. Sci. Semicond. Process. **123**, 105565 (2021)
70. Son, H., Choi, Y.-J., Ha, J.-S., Jung, S.H., Jeon, D.-W.: Crystal quality improvement of α-Ga_2O_3 growth on stripe patterned template via epitaxial lateral overgrowth. Cryst. Growth Des. **19**, 5105–5110 (2019)
71. Cha, A.-N., Bang, S., Rho, H., Bae, H., Jeon, D.-W., Ju, J.-W., et al.: Effects of nanoepitaxial lateral overgrowth on growth of α-Ga_2O_3 by halide vapor phase epitaxy. Appl. Phys. Lett. **115**, 091605 (2019)
72. Son, H., Choi, Y.J., Hong, S.K., Park, J.H., Jeon, D.W.: Reduction of dislocations in alpha-Ga_2O_3 epilayers grown by halide vapor-phase epitaxy on a conical frustum-patterned sapphire substrate. IUCrJ **8**, 462–467 (2021)
73. Kawara, K., Oshima, T., Okigawa, M., Shinohe, T.: In-plane anisotropy in the direction of the dislocation bending in α-Ga_2O_3 grown by epitaxial lateral overgrowth. Appl. Phys. Express **13**, 115502 (2020)
74. Kawara, K., Oshima, Y., Okigawa, M., Shinohe, T.: Elimination of threading dislocations in α-Ga_2O_3 by double-layered epitaxial lateral overgrowth. Appl. Phys. Express **13**, 075507 (2020)
75. Polychroniadis, E., Syväjärvi, M., Yakimova, R., Stoemenos, J.: Microstructural characterization of very thick freestanding 3C-SiC wafers. J. Cryst. Growth **263**, 68–75 (2004)
76. Kumagai, Y., Kubota, Y., Nagashima, T., Kinoshita, T., Dalmau, R., Schlesser, R., et al.: Preparation of a freestanding AlN substrate from a thick AlN layer grown by hydride vapor phase epitaxy on a bulk AlN substrate prepared by physical vapor transport. Appl. Phys. Express **5**, 055504 (2012)
77. Motoki, K., Okahisa, T., Matsumoto, N., Matsushima, M., Kimura, H., Kasai, H., et al.: Preparation of large freestanding GaN substrates by hydride vapor phase epitaxy using GaAs as a starting substrate. Jpn. J. Appl. Phys. **40**, L140 (2001)
78. Ha, M.T., Kim, K.H., Shin, Y.J., Jeong, S.M., Bae, S.Y.: Leidenfrost motion of water microdroplets on surface substrate: epitaxy of gallium oxide via mist chemical vapor deposition. Adv. Mater. Interf. **8**, 2001895 (2021)
79. Uno, K., Ohta, M., Tanaka, I.: Growth mechanism of α-Ga_2O_3 on a sapphire substrate by mist chemical vapor deposition using acetylacetonated gallium source solutions. Appl. Phys. Lett. **117**, 052106 (2020)
80. Hao, J.G., Ma, T.C., Chen, X.H., Kuang, Y., Li, L., Li, J., et al.: Phase tailoring and wafer-scale uniform hetero-epitaxy of metastable-phased corundum α-Ga_2O_3 on sapphire. Appl. Surf. Sci. **513**, 145871 (2020)
81. Ma, T., Chen, X., Ren, F., Zhu, S., Gu, S., Zhang, R., et al.: Heteroepitaxial growth of thick α-Ga_2O_3 film on sapphire (0001) by MIST-CVD technique. J. Semicond. **40**, 012804 (2019)
82. Ma, T.C., Chen, X.H., Kuang, Y., Li, L., Li, J., Kremer, F., et al.: On the origin of dislocation generation and annihilation in α-Ga_2O_3 epilayers on sapphire. Appl. Phys. Lett. **115**, 182101 (2019)
83. Kaneko, K., Nomura, T., Kakeya, I., Fujita, S.: Fabrication of highly crystalline corundum-structured α-$(Ga_{1-x}Fe_x)_2O_3$ alloy thin films on sapphire substrates. Appl. Phys. Express **2**, 075501 (2009)
84. Dang, G.T., Sato, S., Tagashira, Y., Yasuoka, T., Liu, L., Kawaharamura, T.: α-$(Al_xGa_{1-x})_2O_3$ single-layer and heterostructure buffers for the growth of conductive Sn-doped α-Ga_2O_3 thin films via mist chemical vapor deposition. APL Mater. **8**, 101101 (2020)
85. Nishinaka, H., Tahara, D., Morimoto, S., Yoshimoto, M.: Epitaxial growth of α-Ga_2O_3 thin films on a-, m-, and r-plane sapphire substrates by mist chemical vapor deposition using α-Fe_2O_3 buffer layers. Mater. Lett. **205**, 28–31 (2017)

86. Kawaharamura, T., Dang, G.T., Nitta, N.: Atmospheric-pressure epitaxial growth technique of a multiple quantum well by mist chemical vapor deposition based on Leidenfrost droplets. Appl. Phys. Lett. **109**, 151603 (2016)
87. Kim, B., Yang, D., Sohn, W., Lee, S., Jang, T., Yoon, E., et al.: Strain relaxation and dislocation annihilation in compositionally graded α-$(Al_xGa_{1-x})_2O_3$ layer for high voltage α-Ga2O3 power devices. Acta Mater. **221**, 117423 (2021)
88. Jinno, R., Yoshimura, N., Kaneko, K., Fujita, S.: Enhancement of epitaxial lateral overgrowth in the mist chemical vapor deposition of α-Ga_2O_3 by using a-plane sapphire substrate. Jpn. J. Appl. Phys. **58**, 120912 (2019)
89. Dang, G.T., Yasuoka, T., Kawaharamura, T.: Sub-μm features patterned with laser interference lithography for the epitaxial lateral overgrowth of α-Ga_2O_3 via mist chemical vapor deposition. Appl. Phys. Lett. **119**, 041902 (2021)
90. Yang, D., Kim, B., Lee, T.H., Oh, J., Lee, S., Sohn, W., et al.: Selective area growth of single-crystalline alpha-gallium oxide on a sapphire nanomembrane by mist chemical vapor deposition. ACS Appl. Electron. Mater. **3**, 4328 (2021)
91. Lee, S.-D., Akaiwa, K., Fujita, S.: Thermal stability of single crystalline alpha gallium oxide films on sapphire substrates. Phys. Status Solidi (C) **10**, 1592–1595 (2013)
92. Jinno, R., Kaneko, K., Fujita, S.: Thermal stability of α-Ga_2O_3 films grown on c-plane sapphire substrates via mist-CVD. AIP Adv. **10**, 115013 (2020)
93. Guo, D.Y., Zhao, X.L., Zhi, Y.S., Cui, W., Huang, Y.Q., An, Y.H., et al.: Epitaxial growth and solar-blind photoelectric properties of corundum-structured α-Ga_2O_3 thin films. Mater. Lett. **164**, 364–367 (2016)
94. Oshima, T., Kato, Y., Imura, M., Nakayama, Y., Takeguchi, M.: α-Al_2O_3/Ga_2O_3 superlattices coherently grown on r-plane sapphire. Appl. Phys. Express **11**, 065501 (2018)
95. Kracht, M., Karg, A., Feneberg, M., Bläsing, J., Schörmann, J., Goldhahn, R., et al.: Anisotropic optical properties of metastable (01–12) α-Ga2O3 grown by plasma-assisted molecular beam epitaxy. Phys. Rev. Appl. **10**, 024047 (2018)
96. Cheng, Z., Hanke, M., Vogt, P., Bierwagen, O., Trampert, A.: Phase formation and strain relaxation of Ga_2O_3 on c-plane and a-plane sapphire substrates as studied by synchrotron-based X-ray diffraction. Appl. Phys. Lett. **111**, 162104 (2017)
97. Hilfiker, M., Kilic, U., Stokey, M., Jinno, R., Cho, Y., Xing, H.G., et al.: High-frequency and below bandgap anisotropic dielectric constants in α-$(Al_xGa_{1-x})_2O_3$ ($0 \le x \le 1$). Appl. Phys. Lett. **119**, 092103 (2021)
98. Roberts, J.W., Jarman, J.C., Johnstone, D.N., Midgley, P.A., Chalker, P.R., Oliver, R.A., et al.: α-Ga_2O_3 grown by low temperature atomic layer deposition on sapphire. J. Cryst. Growth **487**, 23–27 (2018)
99. Roberts, J.W., Chalker, P.R., Ding, B., Oliver, R.A., Gibbon, J.T., Jones, L.A.H., et al.: Low temperature growth and optical properties of α-Ga_2O_3 deposited on sapphire by plasma enhanced atomic layer deposition. J. Cryst. Growth **528**, 125254 (2019)
100. Massabuau, F.-P., Roberts, J., Nicol, D., Edwards, P., McLelland, M., Dallas, G., et al.: Progress in atomic layer deposited α-Ga_2O_3 materials and solar-blind detectors. Oxide-Based Mater. Devices XII Int. Soc. Optics Photonics **11687**, 116870Q (2021)
101. Wheeler, V.D., Nepal, N., Boris, D.R., Qadri, S.B., Nyakiti, L.O., Lang, A., et al.: Phase control of crystalline Ga_2O_3 films by plasma-enhanced atomic layer deposition. Chem. Mater. **32**, 1140–1152 (2020)
102. Moloney, J., Tesh, O., Singh, M., Roberts, J.W., Jarman, J.C., Lee, L.C., et al.: Atomic layer deposited α-Ga_2O_3 solar-blind photodetectors. J. Phys. D Appl. Phys. **52**, 475101 (2019)
103. Lee, S.H., Lee, K.M., Kim, Y.-B., Moon, Y.-J., Kim, S.B., Bae, D., et al.: Sub-microsecond response time deep-ultraviolet photodetectors using α-Ga_2O_3 thin films grown via low-temperature atomic layer deposition. J. Alloy. Compd. **780**, 400–407 (2019)
104. Schewski, R., Wagner, G., Baldini, M., Gogova, D., Galazka, Z., Schulz, T., et al.: Epitaxial stabilization of pseudomorphic α-Ga_2O_3 on sapphire (0001). Appl. Phys. Express **8**, 011101 (2015)
105. Sun, H., Li, K.-H., Castanedo, C.G.T., Okur, S., Tompa, G.S., Salagaj, T., et al.: HCl flow-induced phase change of α-, β-, and ε-Ga_2O_3 films grown by MOCVD. Cryst. Growth Des. **18**, 2370–2376 (2018)
106. Hou, X., Sun, H., Long, S., Tompa, G.S., Salagaj, T., Qin, Y., et al.: Ultrahigh-performance solar-blind photodetector based on α-phase- dominated Ga_2O_3 film with record low dark current of 81 fA. IEEE Electron Device Lett. **40**, 1483–1486 (2019)
107. Egyenes-Pörsök, F., Gucmann, F., Hušeková, K., Dobročka, E., Sobota, M., Mikolášek, M., et al.: Growth of α- and β-Ga_2O_3 epitaxial layers on sapphire substrates using liquid-injection MOCVD. Semicond. Sci. Technol. **35**, 115002 (2020)
108. Polyakov, A.Y., Smirnov, N.B., Shchemerov, I.V., Yakimov, E.B., Nikolaev, V.I., Stepanov, S.I., et al.: Deep trap spectra of Sn-doped α-Ga_2O_3 grown by halide vapor phase epitaxy on sapphire. APL Mater. **7**, 051103 (2019)
109. Morimoto, S., Nishinaka, H., Yoshimoto, M.: Growth and characterization of F-doped α-Ga2O3 thin films with low electrical resistivity. Thin Solid Films **682**, 18–23 (2019)
110. Sharma, A., Singisetti, U.: Low field electron transport in α-Ga_2O_3: an ab initio approach. Appl. Phys. Lett. **118**, 032101 (2021)
111. Oda, M., Tokuda, R., Kambara, H., Tanikawa, T., Sasaki, T., Hitora, T.: Schottky barrier diodes of corundum-structured gallium oxide showing on-resistance of 0.1 mΩ·cm2 grown by MIST EPITAXY®. Appl. Phys. Express **9**, 021101 (2016)
112. Dang, G.T., Kawaharamura, T., Furuta, M., Allen, M.W.: Mist-CVD grown Sn-doped α-Ga_2O_3 MESFETs. IEEE Trans. Electron Devices **62**, 3640–3644 (2015)
113. Qiao, G., Cai, Q., Ma, T., Wang, J., Chen, X., Xu, Y., et al.: Nanoplasmonically enhanced high-performance metastable phase alpha-Ga_2O_3 solar-blind photodetectors. ACS Appl. Mater. Interf. **11**, 40283–40289 (2019)
114. Bae, J., Jeon, D.-W., Park, J.-H., Kim, J.: High responsivity solar-blind metal-semiconductor-metal photodetector based on α-Ga_2O_3. J. Vac. Sci. Technol. A **39**, 033410 (2021)
115. Yan, X., Shatalov, M., Saxena, T., Shur, M.S.: Deep-ultraviolet tailored-and low-refractive index antireflection coatings for light-extraction enhancement of light emitting diodes. J. Appl. Phys. **113**, 163105 (2013)
116. Ma, S., Feng, S., Kang, S., Wang, F., Fu, X., Lu, W.: A high performance solar-blind detector based on mixed–phase Zn 0.45 Mg 0.55 O alloy nanowires network. Electron. Mater. Lett. **15**, 303–313 (2019)